analytical chemistry

Article

pubs.acs.org/ac

Visualizing the Conversion Process of Alcohol-Induced Fatty Liver to Steatohepatitis in Vivo with a Fluorescent Nanoprobe

Limin Yang, Yuanyuan Chen, Wei Pan, Hongyu Wang, Na Li,* and Bo Tang*

College of Chemistry, Chemical Engineering and Materials Science, Collaborative Innovation Center of Functionalized Probes for Chemical Imaging in Universities of Shandong, Key Laboratory of Molecular and Nano Probes, Ministry of Education, Institute of Molecular and Nano Science, Shandong Normal University, Jinan, Shandong 250014, P. R. China

Supporting Information

ABSTRACT: Excess alcohol consumption and the associated development of alcoholic liver disease (ALD) are major public health challenges worldwide. Since patients with the severe stages of ALD no longer benefit from clinical therapies, early warning of ALD holds significant promise for increasing the cure rate of ALD. Herein, we develop a bicolor fluorescent nanoprobe for dynamically monitoring the conversion process of alcohol-induced fatty liver to steatohepatitis in vivo through simultaneous imaging of microRNA 155 and osteopontin mRNA, which are related to fatty liver and steatohepatitis, respectively. The fluorescence imaging results indicate that the nanoprobe can effectively differentiate alcohol-induced fatty liver and steatohepatitis. Moreover, the nanoprobe can monitor the transmutation process of alcohol-induced fatty liver to steatohepatitis and assess the remission effects of N-acetyl cysteine for alcohol-induced liver injury. We anticipate the developed nanoprobe and imaging method can provide new ways for early warning, treatments, and prognosis of ALD.

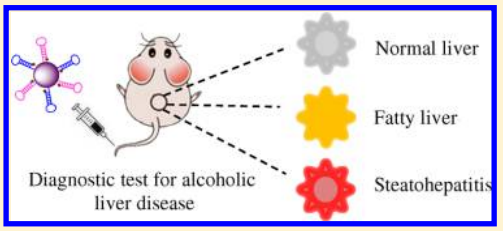

Sustained and excessive alcohol consumption has become one of the main risks for human health.[1−3] Thus, the associated development of alcoholic liver disease (ALD) is a major cause of chronic liver disease and global health-related problems.[4−6] Heavy alcohol intake usually leads to fatty liver, which is the earliest stage of ALD,[7] then worsens to steatohepatitis,[8] and deteriorates to cirrhosis.[9] Eventually, excessive drinking increases the risk of hepatocellular carcinoma (HCC) as well.[10−12] Early stages of ALD, including fatty liver and steatohepatitis, only persist a few months after alcohol withdrawal,[13,14] demonstrating that the ALD can be easily cured if discovered early. Moreover, most patients no longer benefit from clinical therapies at severe stages of ALD, such as cirrhosis and HCC.[15,16] Therefore, detection of ALD at early stages holds great promise for increasing its cure rate. At present, numerous ALD diagnostic methods, including blood biochemistry, histopathological examination, liver biopsy, and ultrasonication, have been developed.[17−21] However, these technologies still possess disadvantages such as poor specificity, a complicated operation process, and high risk. More importantly, these methods can only discriminate alcohol-induced fatty liver or steatohepatitis but are not suitable for monitoring the process from fatty liver to steatohepatitis. Therefore, developing a new strategy for distinguishing alcohol-induced fatty liver and steatohepatitis and real-time visualization of the conversion process of alcohol-induced fatty liver to steatohepatitis is therefore highly desired for early diagnosis and prognosis of ALD.

Recent research has shown that microRNAs and mRNAs are closely associated with ALD and their expression levels are reported to be deregulated in ALD.[22−24] Therefore, the detection of ALD-related RNAs could provide a promising approach for ALD diagnosis.[25,26] However, conventional strategies for ALD-related RNAs detection mainly focus on real-time polymerase chain reaction (RT-PCR), in situ hybridization histochemistry, and microarray analysis, which are usually laborious and sophisticated. Moreover, these methods are not suitable for the detection of RNAs in vivo, which limits their applications in living samples. As a consequence, reliable technologies for in situ visualizing RNAs in vivo with distinct signals are significantly needed for detecting the occurrence and evolvement of ALD.

Fluorescent imaging analysis provides new opportunities to detect and image RNAs due to its excellent charateristics including intuitive visualization and satisfactory temporal and spatial resolution.[27−32] In this regard, we develop a bicolor fluorescent nanoprobe for distinguishing alcohol-induced fatty liver and steatohepatitis, as well as dynamically monitoring the transmutation process of fatty liver to steatohepatitis via in vivo visualization of microRNA 155 (miR-155) and osteopontin mRNA (OPN mRNA). The nanoprobe is designed by decorating the molecular beacons (MBs) onto the surface of gold nanoparticles (AuNPs). Typically, as the fluorescence of fluorophores linked with the MBs was efficiently quenched by AuNPs via fluorescence resonance energy transfer,[33] the corresponding MBs were opened to produce fluorescence signals after interacting with the miR-155 and OPN mRNA, which are biomarkers of alcoholic-induced fatty liver and steatohepatitis, respectively.[34,35] As far as we know, this is the

Received: March 28, 2017
Accepted: May 11, 2017
Published: May 11, 2017

DOI: 10.1021/acs.analchem.7b01144
Anal. Chem. 2017, 89, 6196−6201

first time that a nanoprobe has been used for detecting alcohol-induced fatty liver and steatohepatitis in vivo. The proposed approach can provide a new strategy for early warning and post-treatment evaluation of ALD. The details of this approach are shown in Scheme 1.

Scheme 1. Schematic Illustration of the Nanoprobe for Detection of miR-155 and OPN mRNA (a) and Diagnostic Test for Alcoholic Liver Disease (b)

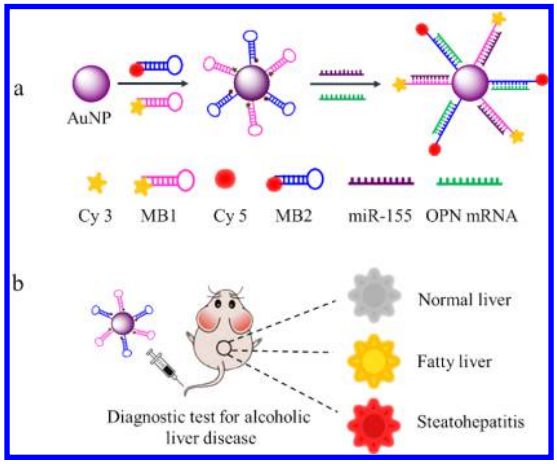

EXPERIMENTAL SECTION

Materials and Instruments. $HAuCl_4 \cdot 4H_2O$, sodium dodecyl sulfate (SDS), trisodium citrate, dithiothreitol (DTT), $MgCl_2$, alcohol, NaCl, and KCl were obtained from China National Pharmaceutical Group Corp. (Shanghai, China). Lipopolysaccharide (LPS) and N-acetyl cysteine (NAC) were purchased from Sigma-Aldrich. Deoxyribonuclease I (DNase I) was obtained from Solarbio Science and Technology Co., Ltd. (Beijing, China). DNA oligonucleotides were synthesized by Sangon Biotechnology Co., Ltd. (Shanghai, China). Detailed DNA sequences and modifications are shown in Table S1.

Fluorescence spectra measurements were taken on a fluorescence spectrometer (Edinburgh, FLS-920). High resolution transmission electron microscopy (HRTEM) was performed on a JEM-2100 electron microscope at an operating voltage of 200 kV (magnification of 200 000×). UV−vis absorption analysis was carried out on a TU-1900 UV−vis spectrometer (Purkinje General, China). RT-PCR was performed with a LineGene 9620 (Bioer, Binjiang, China). The Au content of the samples was measured by inductively coupled plasma atomic emission spectroscopy (ICP-AES, Thermo Fisher, iCAP 7600). Fluorescence animal imaging was acquired with a Caliper IVIS Lumina III imaging system.

Synthesis of Citrate Capped AuNPs. AuNPs were synthesized according to a previous report with some modifications.[36] Typically, by heating 100 mL of $HAuCl_4$ (0.01%) to reflux, 2.0 mL of trisodium citrate (1%) solution was quickly added to the boiling solution under vigorous stirring. After the color of the solution turned to burgundy, the solution was refluxed for an additional 10 min and allowed to cool down to room temperature while stirring. The prepared AuNPs were stored at 4 °C for future use.

Preparation of the Nanoprobe. A 50 nM solution of mixed MB1 and MB2 was added to the AuNPs (1 nM) solution. MB1 and MB2 labeled as Cy3 (sodium 1-[5-(*N*-succinimidyloxycarbonyl)-pent-1-yl]-2-[3-(3,3-dimethyl-1-ethyl-5-sulfonato-indolin-2-ylidene)-1-propen-1-yl]-3,3-dimethyl-3*H*-indolium-5-sulfonate) and Cy5 (sodium 1-[5-(*N*-succinimidyloxycarbonyl)-pent-1-yl]-2-[5-(3,3-dimeth yl-1-ethyl-5-sulfonato-indolin-2-ylidene)-1,3-pentadien-1-yl]-3,3-dimethyl-3*H*-indolium-5-sulfonate)[37] were designed to target miR-155 and OPN mRNA, respectively. After shaking for 4 h at room temperature, the SDS solution with a final concentration of 0.1% was added to the mixture and then left to shake overnight. For the next step, the NaCl solution was added to the above mixture, and its concentration was slowly increased to 0.1 M during an 8 h time period. The resulted solution was aged for an additional 48 h at room temperature after the NaCl addition. The obtained solution was centrifuged at 13 000 rpm for 0.5 h to yield an oily precipitate, which is the nanoprobe. The product was washed with water for three times to rinse off the excess MB1 and MB2 and then stored in the dark at 4 °C until further use. For a comparison study, the nonsense nanoprobe was synthesized under the same procedure but using MB3 and MB4 instead of MB1 and MB2.

DNA Loading Determination. The amount of MBs loaded on the AuNPs was quantified according to a previous report.[38] Specifically, the DTT with 20 mM final concentration was added to the nanoprobe solution (1 nM) under shaking for 12 h to release the MBs. Then, the resulted solution was centrifuged at 13 000 rpm for 30 min. After centrifugation, the released MBs were separated and the fluorescence intensity of the solution was measured. The fluorescence of Cy3-labeled MB1 and Cy5-labeled MB2 was recorded with $\lambda_{ex}/\lambda_{em}$ = 550 nm/565 nm and $\lambda_{ex}/\lambda_{em}$ = 645 nm/665 nm, respectively. The fluorescence intensity was converted to molar concentrations of MBs by interpolation from a standard linear calibration curve. Standard correlation curves were drawn by measuring several MB solutions with known concentrations. The average number of MBs per nanoprobe was determined by dividing the oligonucleotide molar concentration by the AuNPs concentration. All experiments were repeated at least three times for reproducibility.

Kinetics Experiment. The nanoprobe (1 nM) was incubated with miR-155 target (400 nM) and OPN mRNA target (400 nM), respectively. The fluorescence intensity was recorded with increasing time (0, 5, 10, 20, 30, 40, 50, and 60 min). The fluorescence of Cy3 and Cy5 was measured at $\lambda_{ex}/\lambda_{em}$ = 550 nm/565 nm and $\lambda_{ex}/\lambda_{em}$ = 645/665 nm, respectively. All experiments were repeated at least three times.

Hybridization and Specificity Experiments. For miR-155 and OPN mRNA detection, 1 nM of the nanoprobe was incubated with the different concentrations of miR-155 complementary targets and OPN mRNA complementary targets, respectively. After incubation for 1 h at 37 °C, the fluorescence intensities were monitored at appropriate excitation and emission wavelengths. To study the selectivity of the nanoprobe toward miR-155 and OPN mRNA, complementary DNA targets for every MB and other mismatched targets were examined under the same procedure as above.

Stability of the Nanoprobe. The nanoprobe solution (1 nM) was divided into two groups for a comparison study: 2.6 μL of DNase I (1 U/L) was added to one group, and the other was set as the control group. The fluorescence intensities were monitored for 1 h. Afterward, 400 nM DNA targets were added into the two samples with incubation for another 1 h at 37 °C.

DOI: 10.1021/acs.analchem.7b01144
Anal. Chem. 2017, 89, 6196−6201

The fluorescence was recorded with appropriate excitation and emission wavelengths.

RT-PCR. Total liver RNA was isolated using the total RNA Isolation Kit (Promega). cDNA synthesis was performed using an FastQuant RT Kit (Tiangen). RT-PCR was carried out with SuperReal PreMix Plus (Tiangen) on LineGene 9620. Relative expression of OPN mRNA was expressed as the ratio of OPN/actin mRNA levels. First strand synthesis was performed with random primers and reverse transcription with Quant Reverse Transcriptase (Tiangen Biotech, China). RT-PCR of miRNA was carried out with an miRcute miRNA qPCR Detection Kit. Relative level of miRNA was calculated from the quantity of miR-155 PCR products and the quantity of U6 PCR products.

Uptake of the Nanoprobe in Vivo. To confirm the uptake of the nanoprobe in vivo, an approach based on ICP-AES was employed. After the mice were intravenously injected with nanoprobe (50 nM, 200 μL) for 24 h, the organ samples were treated with a mixture of 2 mL of hybrochloric acid (36−38%), 3 mL of nitric acid (65−68%), and 0.5 mL of perchloric acid (70−72%) and then heated to dissolve the AuNPs.

Excretion of the Nanoprobe in Vivo. After the mice were intravenously injected with nanoprobe solution (50 nM, 200 μL) for 24 h, the urine and feces were collected. The urine and the feces were dispersed in the water (0.5 mL) under ultrasonic conditions, respectively. Next, 20 mM of DTT was added to the urine and feces solutions, and then, they were kept shaking for 12 h, resulting in the release of MBs from the nanoprobe. The fluorescence of Cy3-labeled MB1 and Cy5-labeled MB2 was recorded with $\lambda_{ex}/\lambda_{em}$ = 550 nm/565 nm and $\lambda_{ex}/\lambda_{em}$ = 645 nm/665 nm, respectively.

Animal Experiments and in Vivo Imaging Assay. All animal experiments were conducted in accordance with the Principles of Laboratory Animal Care (People's Republic of China) and the Guidelines of the Animal Investigation Committee, Biology Institute of Shandong Academy of Science, China. For alcohol administration, all the mice were aseptically implanted with gastrostomy catheters. The mice were divided into five groups: the first group was infused with water as control group; the second group was infused with an increasing dose of alcohol (22.7 to 35 g/kg per day) for 3 weeks; the third group was also treated similarly to the second group but received a further injection with LPS (10 mg/kg) by the end of the third week; the fourth group was preinfused with NAC (10 mg/kg per day) every morning and then followed by infusing with alcohol (22.7 to 35 g/kg per day) in the afternoon for 3 weeks; the last group was also treated the same way as the fourth group but with an extra dose of NAC (10 mg/kg) and LPS (10 mg/kg) after the end of the third week. Typical fluorescence images were acquired from the mice after intravenous injection of the nanoprobe (50 nM, 200 μL) or the nonsense nanoprobe (50 nM, 200 μL). Before imaging experiments, the mice were anesthetized and fixed in the imaging system. The mice were examined by a Caliper IVIS Lumina III imaging system with 540 nm excitation (Cy3) for miR-155 detection and 620 nm excitation (Cy5) for OPN mRNA detection, respectively. For reactive oxygen species imaging, the mice were intravenous injected with Cy-O-SeH[39] (20 μM, 200 μL) and then anesthetized for fixation before imaging. The mice were examined with 720 nm excitation.

RESULTS AND DISCUSSION

Design and Characterization of the Nanoprobe. To simultaneously detect miR-155 and OPN mRNA, two types of MBs (MB1 and MB2) labeled with Cy3 and Cy5 at their 5′-terminus were used to identify miR-155 and OPN mRNA targets, respectively (Table S1). The dye-labeled probes are used for the RNA determination because they are more suitable than label-free probes[40] for detecting active molecules in vivo. The nanoprobe was prepared via the formation of Au−S between −SH moiety at the 3′-terminus of MBs and AuNPs.[41] AuNPs with a diameter of 20 nm were chose to fabricate the nanoprobe due to its high loading capacity and good quenching ability. HRTEM images show that the sizes of both AuNPs and nanoprobe are consistent at 20 nm (Figure S1). The preparation of the nanoprobe was confirmed by the UV−vis absorption spectra. Figure S2 exhibits the absorption of the AuNPs at 519 nm and the nanoprobe's absorption peak at 524 nm. The red shift of absorption maxima verifies that MBs were successfully modified on the surface of AuNPs.[42] Furthermore, zeta potential experiments demonstrate the zeta potential value of the AuNPs shifted from −14.7 to −18.2 mV after MBs surface modification, suggesting the successful preparation of the nanoprobe. Each AuNP was calculated to be modified by approximately 34 Cy3 labeled MB1 and 35 Cy5 labeled MB2 (Figure S3).

In Vitro Studies of the Nanoprobe. To investigate the feasibility of the nanoprobe for simultaneous detection of the two DNA targets, the fluorescence responses of the nanoprobe upon incubation with perfectly matched DNA targets were performed. As shown in Figure 1, the fluorescent intensities of

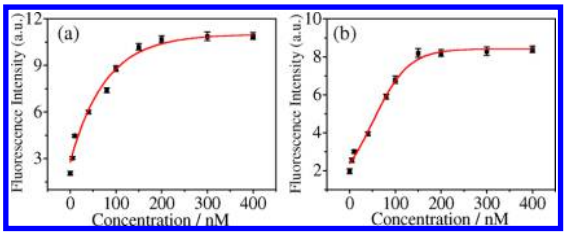

Figure 1. Fluorescence intensity of the nanoprobe in the presence of various concentrations of DNA targets (0−400 nM) measured with different excitation wavelengths, respectively: (a) Cy3 labeled MB1, targeting miR-155, $\lambda_{ex}/\lambda_{em}$ = 550 nm/565 nm. (b) Cy5 labeled MB2, targeting OPN mRNA, $\lambda_{ex}/\lambda_{em}$ = 645 nm/665 nm.

the nanoprobe were enhanced with increasing concentration of the perfectly matched DNA targets, which proves the responses of the nanoprobe toward the DNA targets. However, the fluorescence signal is retained compared with the background in the presence of other mismatched DNA targets (Figure S4). These results suggested that the nanoprobe exhibited remarkable specificity for miR-155 and OPN mRNA, respectively. The kinetic experiment displays the response of the nanoprobe to miR-155 and OPN mRNA targets reaches equilibrium within 0.5 h (Figure S5). Further experiments demonstrate the nanoprobe has significant stability (Figure S6).

Cytotoxicity and Metabolism of the Nanoprobe in Vivo. To evaluate the cytotoxicity of the nanoprobe in vivo, the histological effect of nanoprobe on five major organs (heart, liver, spleen, lung, and kidney) of the mice was studied at 5 days after intravenous injection of a single dose of nanoprobe. As shown in Figure 2, no histopathological abnormalities were found in these tissues, suggesting that the nanoprobe exhibited no cytotoxicity in vivo. It strongly indicated that the nanoprobe was an acceptable candidate to be applied in vivo.

DOI: 10.1021/acs.analchem.7b01144
Anal. Chem. 2017, 89, 6196−6201

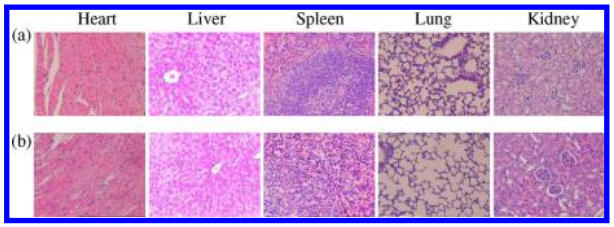

Figure 2. H&E staining images of five major organs (heart, liver, spleen, lung, and kidney) in mice at 5 days for different treatment groups: normal saline (a) and nanoprobe (b).

Since the nanoprobe's excretion behavior is also importance for in vivo applications, the mice's urine and feces analyses were performed. Typically, the urine and feces were collected after the intravenous injection of the nanoprobe in the mice. Meanwhile, the mice with a normal saline injection were used as the control group at the same conditions. As shown in Figure 3, the urine and feces collected from the control mice present

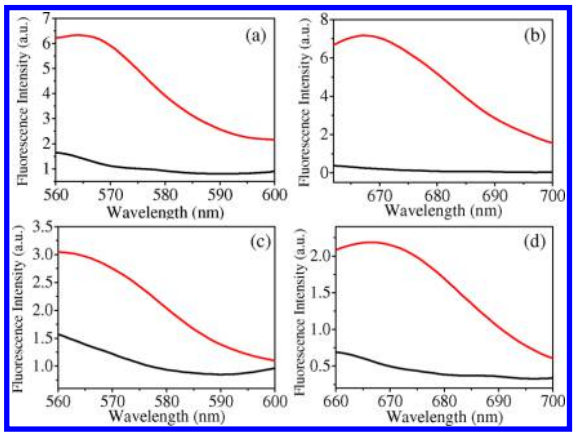

Figure 3. Excretion of nanoprobe in living mice after intravenous injection. Urine (a and b) and feces (c and d) were collected from the mice receiving nanoprobe (red curve) and saline (black curve), respectively. (a and c) λ_{ex} = 550 nm; (b and d) λ_{ex} = 645 nm.

almost no fluorescence signals, while the nanoprobe treated mice display enhanced fluorescence signals. It demonstrates that the nanoprobe can be excreted through the urine and feces. To further confirm the uptake of the nanoprobe in vivo, the Au content at five major organs was studied by ICP-AES after the injection of the nanoprobe in the mice. The results indicate that the contents of Au in liver, heart, spleen, lung, and kidney are 4.1 ± 0.97, 0.19 ± 0.08, 1.17 ± 0.55, 0.12 ± 0.03, and 0.98 ± 0.34 μg/g, respectively. It demonstrates that the nanoprobe is mostly located at the liver region, confirming that the nanoprobe is suitable to visually detect ALD in vivo.

Imaging of the ALD and Remediation in Vivo. For in vivo applications, the nanoprobe was applied to simultaneously visualize the changes of miR-155 and OPN mRNA level in the liver region via fluorescence imaging. The ALD model was constructed using mice which were infused with alcohol to induce fatty liver and further was administered with LPS resulting in steatohepatitis.[34,35] The control group's mice were infused with water only. Liver histologic findings indicate that long-term alcohol feeding induced fatty liver and that further administration with LPS led to steatohepatitis (Figure 4). The other four major organs (heart, spleen, lung, and kidney) in alcohol-treated mice display no histopathological abnormalities (Figure S7), indicating alcohol consumption has no effect on

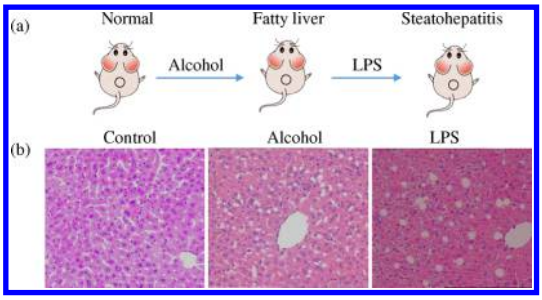

Figure 4. (a) Establishment of ALD model. (b) H&E staining images of liver in mice at control, alcohol, and LPS treatments, respectively.

these other tissues of mice. In order to visualize the degradation process from fatty liver to steatohepatitis, an in vivo imaging system was employed for imaging of the miR-155 and OPN mRNA changes. By the injection of the nanoprobe to the control group, faint fluorescence signals for miR-155 and OPN mRNA were observed in the liver region (Figure 5a,e). As

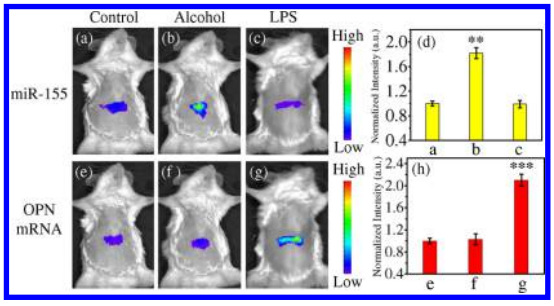

Figure 5. (a–c and e–g) Typical images of the different groups of mice receiving nanoprobe intravenously. The control mice were infused with water. (d, h) The normalized intensities between the experimental groups and control groups. Compared with the control groups, **, $P < 0.01$; ***, $P < 0.001$. All data were shown as mean ± S.D., n = 3 per group.

alcohol-treated mice were injected with the nanoprobe, a strong fluorescence signal for miR-155 and low fluorescence signal for OPN mRNA were observed, demonstrating the existence of fatty liver (Figure 5b,f). When the nanoprobe was injected to LPS-treated fatty liver mice, fluorescence intensities were reduced for miR-155 but enhanced for OPN mRNA compared to the alcohol-treated group (Figure 5c,g), demonstrating that fatty liver was converted to steatohepatitis. Therefore, it validates that the nanoprobe can be applied for monitoring the conversion process from fatty liver to steatohepatitis in vivo.

The conventional technique RT-PCR was further used to detect the variations of miR-155 and OPN mRNA levels. Figure S8 shows that the relative level of miR-155 expression in the livers of alcohol-treated mice is higher than mice of the control group, while the relative level of OPN mRNA is similar. In the meantime, compared with the alcohol-treated mice, miR-155 expression level was reduced but OPN mRNA expression level was enhanced in LPS-treated mice. The strong fluorescence intensities of Cy3 and Cy5 of the nanoprobe suggest that the expression levels of miR-155 and OPN mRNA are high (Figure 5). It demonstrates that the fluorescence signals produced by the nanoprobe are consistent with the levels of miR-155 and OPN mRNA in vivo.

Nonsense nanoprobe, which composes MB3 and MB4 functionalized AuNPs that cannot identify miR-155 and OPN mRNA, was also prepared under the same conditions for

DOI: 10.1021/acs.analchem.7b01144
Anal. Chem. 2017, 89, 6196–6201

comparison study. As shown in Figure S9, the fluorescence intensities of nonsense nanoprobe were not changed while the nanoprobe produced significantly enhanced fluorescence signals in the presence of miR-155 and OPN mRNA. Moreover, the fluorescence signals for miR-155 and OPN mRNA in the livers of alcohol-treated mice and LPS-treated mice were similar to the control group mice by applying the nonsense nanoprobe (Figure 6). These results strongly

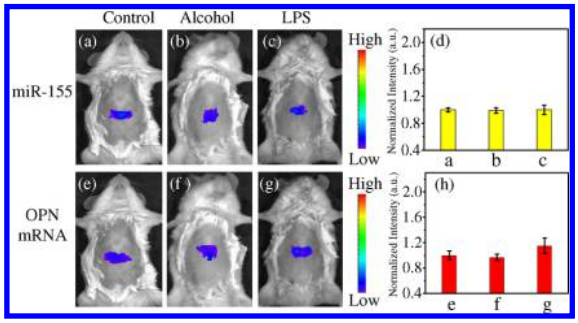

Figure 6. (a–c and e–g) Typical images of the different groups of mice receiving nonsense nanoprobe intravenously. The control mice were infused with water. (d, h) The ratios of fluorescence intensities between the experimental groups and control groups. All data were shown as mean ± S.D., n = 3 per group.

confirmed that the developed nanoprobe has decent specificity for miR-155 and OPN mRNA in vivo. All above results unambiguously prove the capability of the nanoprobe to detect the alterations of miR-155 and OPN mRNA resulting from fatty liver and steatohepatitis, respectively.

Subsequently, the nanoprobe was also explored to visually monitor the remission of alcohol-induced liver damage in vivo. As shown in Figure 7, the fluorescence intensities for miR-155

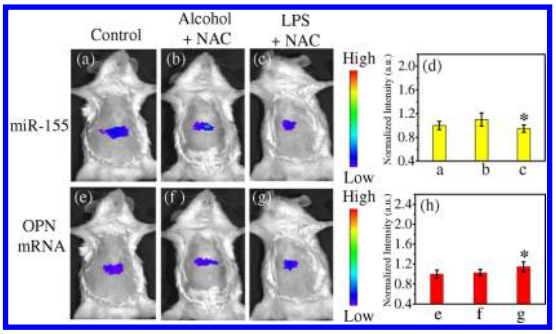

Figure 7. (a–c and e–g) Typical images of the different groups of mice receiving nanoprobe intravenously. The control mice were infused with water. (d, h) The normalized intensities between the experimental groups and control groups. Compared with the control groups, *: $P < 0.05$. All data were shown as mean ± S.D., n = 3 per group.

and OPN mRNA of the nanoprobe were similar to the control group in the NAC treatment. RT-PCR results exhibit consistency with the in vivo imaging experiments (Figure S10). These results demonstrate that the miR-155 and OPN mRNA levels were not changed in the NAC treatment groups. Moreover, liver histological analysis shows that NAC treatment groups display no distinct changes compared with controlled mice (Figure S11). Therefore, these results indicate that NAC can effectively suppress the alcohol-induced liver damage. In addition, the alterations of reactive oxygen species (ROS) were further studied in vivo. Compared with control mice, the fluorescence signals were apparently enhanced in the alcohol-treated mice and LPS-treated mice (Figure S12). Thus, the results revealed that ROS was upregulated in the alcohol-treated mice and also the LPS-treated mice. The strong fluorescence intensity can be effectively attenuated by NAC, indicating that the NAC alleviates alcohol-induced liver damage via reducing the ROS levels in vivo.[43,44] All the results demonstrate that imaging of miR-155 and OPN mRNA in vivo provides a convenient and reliable way to screen new drugs for reducing the alcohol-induced liver damage.

CONCLUSIONS

In summary, a bicolor fluorescent nanoprobe was developed to efficiently detect alcohol-induced fatty liver and steatohepatitis by simultaneously imaging miR-155 and OPN mRNA in vivo. With remarkable specificity, outstanding biocompatibility, and easy excretion, the nanoprobe can be well-suited as a fluorescent imaging tool for monitoring the transformation process of fatty liver to steatohepatitis and evaluating remission effects of NAC for alcohol-induced liver damage as well. To the best of our knowledge, this is the first time that a nanoprobe has been used for detection of the occurrence and development of ALD. The current imaging method provides a new way to obtain reliable information for early warning and treatment of ALD. Hence, the imaging of major disease-related markers in vivo will be a promising strategy for drug screening and precise treatment of such diseases.

ASSOCIATED CONTENT

Supporting Information

The Supporting Information is available free of charge on the ACS Publications website at DOI: 10.1021/acs.analchem.7b01144.

DNA sequences, TEM images, UV–vis spectra, specificity, kinetics studies, stability, H&E staining images, representative fluorescence images, and RT-PCR results (PDF)

AUTHOR INFORMATION

Corresponding Authors

*Fax: (86)-531-86180017. E-mail: lina@sdnu.edu.cn.
*Fax: (86)-531-86180017. E-mail: tangb@sdnu.edu.cn.

ORCID

Bo Tang: 0000-0002-8712-7025

Notes

The authors declare no competing financial interest.

ACKNOWLEDGMENTS

This work was supported by 973 Program (2013CB933800), National Natural Science Foundation of China (21390411, 21535004, 21422505, 21375081, 21505087), and Natural Science Foundation for Distinguished Young Scholars of Shandong Province (JQ201503).

REFERENCES

(1) Louvet, A.; Mathurin, P. *Nat. Rev. Gastroenterol. Hepatol.* **2015**, *12*, 231–242.
(2) Rehm, J.; Samokhvalov, A. V.; Shield, K. D. *J. Hepatol.* **2013**, *59*, 160–168.
(3) Boban, M.; Stockley, C.; Teissedre, P. L.; Restani, P.; Fradera, U.; Stein-Hammer, C.; Ruf, J. C. *Food Funct.* **2016**, *7*, 2937–2942.

DOI: 10.1021/acs.analchem.7b01144
Anal. Chem. 2017, 89, 6196–6201

(4) Wang, F. S.; Fan, J. G.; Zhang, Z.; Gao, B.; Wang, H.-Y. *Hepatology* **2014**, *60*, 2099−2108.
(5) Altamirano, J.; Bataller, R. *Nat. Rev. Gastroenterol. Hepatol.* **2011**, *8*, 491−501.
(6) Barve, A.; Marsano, L. S.; Parajuli, D.; Cave, M.; McClain, C. J. *Liver Disorders*; Springer International Publishing: Cham, 2017; pp 173−197.
(7) O'shea, R. S.; Dasarathy, S.; McCullough, A. *Hepatology* **2010**, *51*, 307−328.
(8) Mathurin, P.; Louvet, A.; Dharancy, S. *Gastroenterol. Clin. Biol.* **2008**, *32*, S179−S181.
(9) Pessione, F.; Ramond, M. J.; Peters, L.; Pham, B.-N.; Batel, P.; Rueff, B.; Valla, D.-C. *Liver Int.* **2003**, *23*, 45−53.
(10) Marrero, J. A.; Fontana, R. J.; Fu, S.; Conjeevaram, H. S.; Su, G. L.; Lok, A. S. *J. Hepatol.* **2005**, *42*, 218−224.
(11) McKillop, I. H.; Schrum, L. W. *Alcohol* **2005**, *35*, 195−203.
(12) Zhong, S. *Cancer Res.* **2016**, *76*, 4936−4936.
(13) Takahashi, H.; Ono, M.; Hyogo, H.; Tsuji, C.; Kitajima, Y.; Ono, N.; Eguchi, T.; Fujimoto, K.; Chayama, K.; Saibara, T.; Anzai, K.; Eguchi, Y. *J. Gastroenterol.* **2015**, *50*, 1114−1123.
(14) Lucey, M. R.; Mathurin, P.; Morgan, T. R. *N. Engl. J. Med.* **2009**, *360*, 2758−2769.
(15) Poon, R. T. P.; Fan, S. T.; Wong, J. *Ann. Surg.* **2000**, *232*, 10−24.
(16) Farazi, P. A.; DePinho, R. A. *Nat. Rev. Cancer* **2006**, *6*, 674−687.
(17) Bhagwandeen, B. S.; Apte, M.; Manwarring, L.; Dickeson, J. *J. Pathol.* **1987**, *152*, 47−53.
(18) Chen, Y.; Singh, S.; Matsumoto, A.; Manna, S. K.; Abdelmegeed, M. A.; Murphy, G. S.; Dong, H.; Song, B.−J.; Gonzalez, F. J.; Thompson, D. C.; Vasiliou, V. *Sci. Rep.* **2016**, *6*, 29743.
(19) Bravo, A. A.; Sheth, S. G.; Chopra, S. *N. Engl. J. Med.* **2001**, *344*, 495−500.
(20) Poynard, T.; Aubert, A.; Bedossa, P.; Abella, A.; Naveau, S.; Paraf, F.; Chaput, J. C. *Gastroenterology* **1991**, *100*, 1397−1402.
(21) Xu, T.; Zheng, L.; Xu, L.; Yin, L.; Qi, Y.; Xu, Y.; Han, X.; Peng, J. *Arch. Toxicol.* **2014**, *88*, 739−753.
(22) Yeligar, S.; Tsukamoto, H.; Kalra, V. K. *J. Immunol.* **2009**, *183*, 5232−5243.
(23) Dolganiuc, A.; Petrasek, J.; Kodys, K.; Catalano, D.; Mandrekar, P.; Velayudham, A.; Szabo, G. *Alcohol.: Clin. Exp. Res.* **2009**, *33*, 1704−1710.
(24) Avissar, M.; McClean, M. D.; Kelsey, K. T.; Marsit, C. J. *Carcinogenesis* **2009**, *30*, 2059−2063.
(25) Bala, S.; Petrasek, J.; Mundkur, S.; Catalano, D.; Levin, I.; Ward, J.; Alao, H.; Kodys, K.; Szabo, G. *Hepatology* **2012**, *56*, 1946−1957.
(26) Zhang, Y.; Jia, Y.; Zheng, R.; Guo, Y.; Wang, Y.; Guo, H.; Fei, M.; Sun, S. *Clin. Chem.* **2010**, *56*, 1830−1838.
(27) Fernández-Suárez, M.; Ting, A. Y. *Nat. Rev. Mol. Cell Biol.* **2008**, *9*, 929−943.
(28) Zhao, X.; Xu, L.; Sun, M.; Ma, W.; Wu, X.; Kuang, H.; Wang, L.; Xu, C. *Small* **2016**, *12*, 4662−4668.
(29) Yang, L.; Ren, Y.; Pan, W.; Yu, Z.; Tong, L.; Li, N.; Tang, B. *Anal. Chem.* **2016**, *88*, 11886−11891.
(30) Li, S.; Xu, L.; Ma, W.; Wu, X.; Sun, M.; Kuang, H.; Wang, L.; Kotov, N. A.; Xu, C. *J. Am. Chem. Soc.* **2016**, *138*, 306−312.
(31) Luan, M.; Li, N.; Pan, W.; Yang, L.; Yu, Z.; Tang, B. *Chem. Commun.* **2017**, *53*, 356−359.
(32) Li, S.; Xu, L.; Sun, M.; Wu, X.; Liu, L.; Kuang, H.; Xu, C. *Adv. Mater.* **2017**, *29*, 1606086.
(33) Ray, P. C.; Fortner, A.; Darbha, G. K. *J. Phys. Chem. B* **2006**, *110*, 20745−20748.
(34) Bala, S.; Szabo, G. *Int. J. Hepatol.* **2012**, *2012*, 498232.
(35) Banerjee, A.; Burghardt, R. C.; Johnson, G. A.; White, F. J.; Ramaiah, S. K. *Toxicol. Pathol.* **2006**, *34*, 373−384.
(36) Grabar, K. C.; Freeman, R. G.; Hommer, M. B.; Natan, M. J. *Anal. Chem.* **1995**, *67*, 735−743.
(37) Hahn, C. D.; Riener, C. K.; Gruber, H. J. *Single Mol.* **2001**, *2*, 149.
(38) Pan, W.; Zhang, T.; Yang, H.; Diao, W.; Li, N.; Tang, B. *Anal. Chem.* **2013**, *85*, 10581−10588.
(39) Xu, K.; Qiang, M.; Gao, W.; Su, R.; Li, N.; Gao, Y.; Xie, Y.; Kong, F.; Tang, B. *Chem. Sci.* **2013**, *4*, 1079−1086.
(40) Wang, M.; Wang, W.; Kang, T. S.; Leung, C. H.; Ma, D. L. *Anal. Chem.* **2016**, *88*, 981−987.
(41) Rosi, N. L.; Giljohann, D. A.; Thaxton, C. S.; Lytton-Jean, A. K. R.; Han, M. S.; Mirkin, C. A. *Science* **2006**, *312*, 1027−1030.
(42) Li, N.; Chang, C.; Pan, W.; Tang, B. *Angew. Chem., Int. Ed.* **2012**, *51*, 7426−7430.
(43) Ozaras, R.; Tahan, V.; Aydin, S.; Uzun, H.; Kaya, S.; Senturk, H. *World J. Gastroenterol.* **2003**, *9*, 125−128.
(44) Moreno, C.; Langlet, P.; Hittelet, A.; Lasser, L.; Degré, D.; Evrard, S.; Colle, I.; Lemmers, A.; Devière, J.; Le Moine, O. *J. Hepatol.* **2010**, *53*, 1117−1122.

DOI: 10.1021/acs.analchem.7b01144
Anal. Chem. 2017, 89, 6196−6201